ANNALI DI GEOFISICA, VOL. XXXVI, N. 1, April 1993

Fault rupture geometry for the 1980 Irpinia earthquake: a working hypothesis

Rob Westaway
Department of Geological Sciences, University of Durham, England

Abstract
The fault rupture nucleation point of the Irpinia earthquake is relocated, following the recent identification of ~20 km of surface faulting, the Carpineta and Picentini fault scarps, in addition to the ~15 km previously documented on the Marzano and San Gregorio faults, all of which have northwestward strike and ~60° northeastward dip. This relocation, relative to a well-located aftershock, is based on detailed analysis of *Pn*-wave arrival times at permanent seismograph stations. It indicates a range of revised origin times and nucleation point positions at (10÷12) km depth that are ~(5÷9) km southeast of previously documented coordinates, between 18:34:52.0 ± 0.3 s, with latitude 40.724° ± 1.4 km and longitude 15.414° ± 1.4 km (preferred), and 18:34:52.5 ± 0.3 s, with latitude 40.742° ± 1.4 km and longitude 15.373° ± 1.4 km. The preferred nucleation point coincides with a downdip projection of the southeast end of the Carpineta fault and indicates that this fault ruptured first, rather than the Marzano fault as was previously thought.
With fault rupture nucleation point adjusted to this new preferred position, field and seismological estimates of seismic moment match well, both overall and for individual fault scarps, and suggest the following sequence of fault ruptures. The initial fault rupture nucleated at or near the southeast end of the Carpineta fault and propagated northwest, releasing ~2.5×10^{18} Nm seismic moment. Rupture continued apparently without interruption onto the adjoining Marzano fault, where ~6.5×10^{18} Nm of seismic moment was released. Rupture then paused for ~0.5 s, before continuing northwestward along the Picentini fault, where ~4.5×10^{18} Nm more seismic moment was released. About 14 s after this sequence of NW-propagating ruptures began, a SE-propagating rupture released ~2×10^{18} Nm seismic moment on the San Gregorio fault. Each of these ruptures was associated with surface faulting and intense aftershock activity. The existence of another aftershock cluster northwest of the Picentini scarp suggests a fifth fault rupture, at Castelfranci, which released up to ~2×10^{18} Nm more seismic moment. Faulting at this locality ~12 s after the initial rupture began also appears necessary to explain the form of ground acceleration recorded nearby.
Two additional ruptures occurred on faults with different orientations, ~20 s and ~40 s after the initial rupture. The 40 s subevent involved the release of ~3×10^{18} Nm of seismic moment on a steep normal fault that dips southwest at ~70° and reaches the Earth's surface ~11 km northeast of the Marzano fault. The 20 s subevent apparently involved the release of ~4×10^{18} Nm of seismic moment on a surface dipping northeast at ~20°, at the base of the brittle upper crust beneath this steep antithetic fault.
Points where ruptures nucleated on the steep NE-dipping normal faults coincide with *en echelon* steps of ~1 km and abrupt ~15° changes in strike. The Marzano and Carpineta faults, which have strike ~315°, took up a small component of left-lateral slip, as is revealed by the first-motion focal mechanism, teleseismic waveform modelling, striations measured in the field, and consistent rightward stepping: their slip vector azimuth is ~N37°E. Assuming the same slip vector azimuth, a component of right-lateral slip is expected on the San Gregorio and Picentini faults that have strike ~300°.

1. Introduction

The Irpinia earthquake of 23 November 1980 was the largest (surface-wave magnitude M_S = 6.9; seismic moment $M_0 = 26 \times 10^{18}$ Nm) normal-faulting event in the Apennine mountains of Italy for over 60 y. Because normal-faulting earthquakes of this size are relatively rare, studies

of this event contribute not only to the knowledge of the active tectonics of Italy, but also to the understanding of continental extension in general.

Westaway and Jackson (1987) published a set of results concerning this earthquake that documented information then available. These included, first, results of location studies (table I), and a description of ~15 km of surface faulting, the Marzano and San Gregorio fault scarps, with ~60° northeastward dip and northwestward strike, which had earlier been reported by Westaway and Jackson (1984). Second, we (1987) attempted forward modelling of long-period teleseismic waveforms, with the aim of correlating seismogram complexity with observed complexity of surface faulting and other structure in the epicentral region. We suggested that an initial rupture on the Marzano fault was followed by the rupture of the San Gregorio fault ~12.8 s later. This waveform modelling also established that additional faulting probably occurred which had not then been identified at the Earth's surface. Third, we examined records of ground acceleration from the epicentral region, attempting to use their timing to constrain the relative positions of two later fault ruptures (which occurred ~20 s and ~40 s after rupture initiated) more tightly than was possible from teleseismic observations. We suggested that these two late subevents involved rupture on very low-angle surfaces at the base of the upper crustal brittle layer, with dip ~20° to the northeast. We also considered the 1980 aftershock sequence in detail, showing that it persisted northwestward well beyond the documented surface faulting. This aftershock activity included a dense cluster more than ~20 km northwest of the documented surface faulting (Westaway and Jackson, 1987, fig. 23a)) near Castelfranci, which had more northerly trend (~330°) than the rest of the aftershock zone. No aftershock had magnitude > ~5, and the cumulative deformation associated with aftershocks was negligible. All surface faulting was thus almost certainly produced by the mainshock. Finally, we discussed observations of the elevation change that were obtained by relevelling following the earthquake and were first documented by Arca *et*

Table I. Locations of the mainshock nucleation point and the aftershock used as master event.

Time	Latitude (°)	Longitude (°)	Depth	N.	Ref
		Mainshock nucleation point; 23 November 1980			
18:34:53.8	40.9	15.4	10 (fixed)	265	NEIS
18:34:52.2 ± 0.1	40.86 ± 1.4	15.33 ± 1.1	0 (fixed)	506	ISC
18:34:52.8 ± 0.3	40.762 ± 2.4	15.332 ± 2.5	15.2 ± 2.6	32	WJ87 (3)
± 0.1	40.778 ± 1.7	15.332 ± 1.6	(12) (fixed)	63	WJ87 (4)
18:34:52.0 ± 0.3	40.724 ± 1.4	15.414 ± 1.4	12 ± 2	46	This study A
18:34:52.5 ± 0.3	40.742 ± 1.4	15.373 ± 1.4	12 ± 2	46	This study B
		Aftershock; 8 December 1980 (m_b 4.6)			
02:49:39.6	40.9	15.3	10 (fixed)		NEIS
02:49:40.1 ± 0.34	40.88 ± 3.5	15.29 ± 3.4	10 (fixed)	81	ISC
02:49:40.0 ± 0.1	40.805 ± 0.8	15.229 ± 0.8	12 ± 2	27	WJ87
02:49:40.0 ± 0.3	40.805 ± 0.8	15.229 ± 0.8	12 ± 2	27	This study

NEIS, ISC, and WJ87 denote bulletins of the US National Earthquake Information Service and the International Seismological Centre, and Westaway and Jackson (1987). Note that the aftershock origin time was listed incorrectly by WJ87: the correct time, from Appendix G of Westaway (1985), is quoted here. The aftershock location from this study is derived from that by WJ87; uncertainty in latitude and longitude δx_i (i=1,2) are retained as before, though the estimated uncertainty in origin time is increased following the discussion in the text. Mainshock locations A and B are derived from the relative locations obtained by fitting curves A and B to the data in fig. 2b), taking account of the preferred aftershock location. For each of these, listed nominal uncertainty in origin time δT_0 is the same as for the aftershock, and uncertainty in position is calculated, assuming errors in aftershock position and origin time are uncorrelated, as the square root of $(2\ \delta T_0 / v_m)^2 + \delta x_i^2$.

al. (1983). Westaway (1987b) had already shown that part of this data set was unreliable, with the elevation change caused by landsliding and not by tectonic deformation.

Subsequent studies have increased the understanding of some aspects of this earthquake far beyond what we (1987) achieved.

Pantosti and Valensise (1990a) reported ~20 km of additional surface faulting, much of which was along the front of the Picentini range (Westaway and Jackson, 1987, plate 1) where we (1984, 1987) had predicted it. Pantosti and Valensise (1990b) presented results of trenching across the Marzano scarp that establish ~1700 y recurrence for earthquakes similar to the 1980 event. This recurrence history is shared by the San Gregorio fault, and presumably also by the intervening Carpineta fault. Documented local historical earthquakes that were comparable to the 1980 event, as in 1694 and 990 (see, *e.g.*, Westaway and Jackson, 1987, fig. 26; Postpischl, 1985), thus did not rupture these faults. Bernard and Zollo (1989) proposed different relative timings and positions of the initial rupture and the 20 s and 40 s subevents (table II). Their position for the 40 s subevent was not far from ours – ~10 km northeast of the Marzano fault scarp – but they suggested instead that it occurred on a steep antithetic normal fault dipping southwest. A source with this orientation has a far-field (teleseismic) radiation pattern similar to the one that we (1987) proposed for this subevent. However, their (1989) near-field seismological studies, which could resolve this nodal plane ambiguity, established that the relatively steep plane dipping southwest was the fault plane. Pantosti and Valensise (1990a) reached a similar conclusion, which I now accept, following elastic dislocation modelling of the portion of the elevation change data set from near this locality, which they considered reliable.

The same degree of certainty cannot be said to have been reached by investigations of the 20 s subevent. Bernard and Zollo (1989) proposed a radically different position from us (1987): ~20 km southeast of our (1987) fault rupture nucleation point. They suggested that this subevent caused the surface faulting near San Gregorio.

Table II. Observations of timing of seismic phases on strong-motion records.

Stn		S_0 (s)	P_{40} (s)	S_{40} (s)	S_{40}–P_{40} (s)	R_{40} (km)	S_{40}–S_0 (s)	R_{40}–R_0 (s)
BAG	WJ	3.0 ± 0.2	38.5 ± 0.2	43.4 ± 0.2	4.9 ± 0.4	40.6 ± 3.3	40.4 ± 0.4	
	BZ	2.6 ± 0.2	(38.5 ± 0.2)	41.9 ± 0.2	3.4 ± 0.4	28.2 ± 3.3	39.3 ± 0.4	–2.5 ± 1.4
BIS	WJ	4.7 ± 0.4	38.3 ± 0.2	40.8 ± 0.3	2.5 ± 0.5	17.8 ± 3.6	36.1 ± 0.7	
	BZ	5.3 ± 0.3	38.0 ± 0.1	(40.8 ± 0.3)	2.8 ± 0.4	19.9 ± 2.8	35.5 ± 0.6	–13.5 ± 1.8
BOV	BZ	4.8 ± 0.5		42.4 ± 2.0			37.6 ± 2.5	–8.4 ± 8.8
CAL	WJ	3.7 ± 0.4	38.8 ± 0.4	40.1 ± 0.2	2.3 ± 0.6	16.4 ± 4.3	36.4 ± 0.6	
	BZ	4.2 ± 0.2	38.7 ± 0.2	40.2 ± 0.1	2.5 ± 0.3	17.8 ± 2.1	36.0 ± 0.3	–12.0 ± 1.6
MER	BZ	5.5 ± 0.3		46.0 ± 1.0			40.5 ± 1.3	+1.5 ± 3.9
RIO	WJ		40.0 ± 0.5	44.0 ± 0.5	4.0 ± 1.0	28.4 ± 7.1		
	BZ	5.0 ± 0.5		43.8 ± 1.0			38.8 ± 1.5	–3.6 ± 3.8
STU	WJ	4.0 ± 0.3		42.2 ± 0.3			38.2 ± 0.6	–6.3 ± 1.2
	BZ	2.3 ± 0.2		42.2 ± 0.2			39.9 ± 0.4	

Stn denotes the accelerograph station, from Bernard and Zollo (1989): BAG is Bagnoli Irpino, BIS is Bisaccia, BOV is Bovino, CAL is Calitri, MER is Mercato San Severino, RIO is Rionero in Vulture, and STU is Sturno. S_0 is the observed *S*-wave arrival time (after trigger time) for the initial fault rupture. P_{40} and S_{40} are observed *P*-wave and *S*-wave arrival times (after trigger time) for the 40 s fault rupture. R_{40} is the hypocentral distance to the 40 s source, estimated as $R_{40}=(S_{40}-P_{40})\ V_S\ \gamma/(\gamma-1)$, where V_S is the *S*-wave velocity and γ is the ratio of *P*-wave velocity to *S*-wave velocity. For γ I use 1.73; for V_S I use 3.0 km s^{-1} for BIS, CAL, and RIO and 3.5 km s^{-1} at other stations. This assumed lateral variation in *S*-wave velocity is roughly consistent with the suggestion by Bernard and Zollo (1989) that seismic velocities are typically slower northeast of the epicentral area. Values of R_{40}–R_0 are estimated from S_{40}–S_0 assuming the 40 s subevent initiated precisely 40 s after the initial subevent.

However, because this faulting had ~60° northeastward dip at the Earth's surface (Westaway and Jackson, 1984, 1987), they were obliged to conclude that this fault flattened to 20° dip at shallow depth to explain our (1987) teleseismic waveform modelling. They suggested that this lower dip is supported by elastic dislocation modelling of elevation changes near their suggested position of this fault plane. However, recalling the problems that exist elsewhere with this elevation change data set (Westaway, 1987; Pantosti and Valensise, 1990a), it appears unwise to have faith in it without supporting evidence, particularly since no one appears to have scrutinised the reliablility of the part of it near San Gregorio.

Furthermore, it is difficult to explain why the San Gregorio fault should be strongly listric when others along strike from it are planar, with ~60° dip, to the base of the brittle upper crust (Westaway and Jackson, 1987, Pantosti and Valensise, 1990a). Finally, aftershock activity was negligible near much of Bernard and Zollo's (1989) suggested 20° dipping fault plane, indicating that a major fault with this position and orientation is most unlikely to have ruptured in the mainshock. In contrast, the compact width in the NE direction of the aftershock cluster near San Gregorio (Westaway and Jackson, 1987) indicates strongly that the fault that ruptured there was very steep throughout the brittle layer. Bernard and Zollo (1989) located this subevent relative to the 40 s subevent using *S*-wave arrivals recorded at accelerograph stations. However, they could identify arrivals at only three accelerograph stations, Brienza, Auletta, and Tricarico (see their fig. 13). The lack of clarity of these arrivals and the dissimilarity of their form at different stations do not inspire confidence that they (1989) necessarily picked the same seismic phase in all three cases.

This *S*-wave is clear only at Brienza, where their (1989) arrival time ((9.5 ± 0.2) s after the instrument triggered) is similar to ours (9 s) for our (1987) subevent ~12.8 s, not ~20 s, after the initial fault rupture. The main cause of differences between timing interpretations is their (1989) use of a slower velocity structure for calculating travel times. We (1987) assumed the average *S*-wave velocity to be 3.5 km s^{-1}, typical for well-consolidated crustal rock. They used a complex layered velocity model with lower *S*-wave velocities throughout the top 10 km, with the very low value of 1.26 km s^{-1} in the top 3 km. Such a low velocity would be expected in unconsolidated sediment, and it is difficult to justify it for the Mesozoic crystalline limestone that crops out in much the 1980 epicentral area. Their (1989) velocity structure causes *S*-wave travel times ~3 s greater than ours (1987) for propagation from a ~10 km deep source to a station at ~30 km distance. For example, their (1989) *S*-wave travel time for the 49 km distance to Brienza from their preferred location for the 40 s subevent is 17.7 s, whereas assuming the *S*-wave velocity to be 3.5 km s^{-1} it would be only 14 s.

Although they noted some of these problems, Pantosti and Valensise (1990a) nonetheless accepted that the 20 s subevent that we (1987) identified teleseismically fitted the interpretation by Bernard and Zollo (1989) and therefore probably was associated with the San Gregorio scarp. Their view (which I support) that this fault is steep, if combined with this suggested position for the 20 s subevent that we (1987) observed teleseismically (which I do not support), requires the conclusion that our (1987) teleseismic waveform modelling is incapable of distinguishing 20° from 60° northeastward dip. However, assuming the shear modulus to be 30 GPa, the 4×10^{18} Nm seismic moment observed teleseismically in the 20 s subevent (Westaway and Jackson, 1987) would require ~2 m average coseismic slip, given the <~7 km length of the San Gregorio scarp (Pantosti and Valensise, 1990a), its 60° dip, and its ~10 km vertical extent.

Elastic dislocation modelling of coseismic deformation (*e.g.*, Ward and Barrientos, 1986; Pantosti and Valensise, 1990a) suggests that, for a 60° dipping normal fault, slip at the Earth's surface is roughly half that at depth. The 1 m scarp at the Earth's surface on the Marzano fault indeed appears to have been caused by ~2 m *maximum* slip at depth (Pantosti and Valensise, 1990a). However, it is difficult to reconcile the ~0.5 m high scarp observed at the Earth's surface at San Gregorio with 2 m *average* slip at depth, which would be required if 4×10^{18} Nm seismic moment was released on the San Gregorio fault.

In addition, the teleseismic radiation from the

20 s subevent shows strong azimuthal variations in amplitude, and is of unusually long duration (> ~8 s), both of which appear diagnostic of low-angle rupture at the base of the brittle layer (Eyidogan and Jackson, 1985). Furthermore, the relatively low ground acceleration for the 20 s subevent in relation to its seismic moment (Westaway and Jackson, 1987) suggests that it may have involved unusual source physics, perhaps associated with relatively slow downward propagation of a rupture into the usually plastic uppermost lower crust. The 40 s subevent, in contrast, showed shorter source duration (~4 s), and was always the weaker candidate for a very low-angle rupture.

Panza and Suhadolc (1989) also suggested that a rupture occurred near San Gregorio ~20 s after the initial rupture nucleated. Inclusion of this rupture had a dramatic effect on their synthetic accelerograms at Auletta and Brienza. However, these synthetic accelerograms bear little resemblence to those observed at these stations. Their (1989) timing scheme for the accelerograms also differs in detail from that by Bernard and Zollo (1989). Harabaglia *et al.* (1990) proposed also another timing scheme for the accelerograms.

Despite this controversy concerning some source parameters for the Irpinia earthquake, some of our other (1987) parameters have apparently been accepted without question. One of the most important is our preferred position for the fault rupture nucleation point (location 4 in table I), which was obtained relative to one of the larger aftershocks that was located to high precision using data from a dense temporary network of portable seismographs that was deployed after the mainshock. The main purpose of this article, as described in sect. **2**, is to demonstrate that a revised location method along with more careful scrutiny of the available *P*-wave arrival time data gives a significantly different nucleation point. The implications of this result are discussed in sect. **3**. One major implication is that the San Gregorio fault began to rupture (14÷16) s after the initial rupture, slightly later than the ~12.8 s timing suggested by us (1987). The 20 s subevent observed teleseismically is thus different, and has nothing to do with the San Gregorio fault.

2. Nucleation point of the initial fault rupture

2.1. *Review of previous locations*

I am unaware of any study that has independently located the fault rupture nucleation point of the Irpinia earthquake since Westaway and Jackson (1987), or even of any that has checked our (1987) results. Our preferred (1987) location used a relative location procedure by Westaway (1987a) that assumes the master and secondary events occurred at the same focal depth (or that any difference in their focal depths is small compared with their separation). We (1987) suggested that the initial rupture in the 1980 mainshock nucleated probably at ~12 km depth, at the base of the brittle layer, and had centroid depth ~10 km, indicating a component of upward rupture propagation. Locations of the mainshock nucleation point and the aftershock used as a master event, including those from agency bulletins and from our (1987) results, are listed in table I.

Routine agency locations for both the mainshock and this aftershock are ~10 km north of the locations suggested by local studies. This systematic error is caused by the uneven station distribution, and is a well-established problem for many agency locations of Mediterranean earthquakes (see, *e.g.* Westaway and Jackson, 1987): most permanent seismograph stations are to the north or northwest on the focal sphere (see, *e.g.*, fig. 3 of Westaway and Jackson, 1987). Origin time, focal depth, and latitude trade off strongly between the different locations. The low formal standard errors for our (1987) aftershock epicentre, ~0.8 km, reflect the large number of seismographs in the temporary network (37), most of which (27) recorded this event, the use of some (7) *S*-wave arrival time data, and the use of station corrections to partially account for lateral variations in structure beneath different stations. This aftershock location is potentially questionable given that it was not obtained using a proper three-dimensional velocity model. However, the principal lateral variation in the velocity structure in the epicentral area is the relative slowness of velocity northeast of the 1980 surface faulting, compared with other azimuths, which if not corrected will cause aftershock loca-

tions to be too far southwest (Bernard and Zollo, 1989). This may offset the resulting relative location of the mainshock southwest of its true position. However, the main issue that I am pursuing here is the uncertainty in location of the 1980 mainshock relative to this aftershock. Because of the independence of the methods used, this is independent of uncertainty in the aftershock location. Furthermore, the principal contention, which concerns the southeastward separation of the mainshock and aftershock, is independent of any northeastward mislocation of the aftershock caused by any failure to account for the principal lateral variation in the velocity structure in the epicentral area.

The International Seismological Centre (ISC) aftershock location is ~10 km northnortheast of our (1987) location, and has origin time 1.3 s later (table I). Our (1987) aftershock location was obtained using a velocity model in which velocity increased linearly with depth. The typical ray geometry for this structure (see fig. 3.2.4 of Westaway, 1985) means that rays leaving a source at 10 km depth to stations within ~34 km epicentral distance will take off upward. Given the ~60 km diameter of the temporary seismograph network (see fig. 3.1.1 of Westaway, 1985), and given that the epicentre of the aftershock used as a master event was near the centre of this network, rays to most stations that recorded this aftershock took off upwards. This means that if its depth were adjusted shallower from 12 to say 10 km, the origin time obtained using this temporary network would adjust slightly later. The later ISC origin time is explained by the higher latitude of their epicentre, which is nearer most permanent seismograph stations that recorded the aftershock. Overall, taking all these observations into account, the depth of this aftershock can be conservatively assessed as ~(10÷12) km, and its origin time appears to have been within ~±0.3 s of 02:49:40 on 8 December 1980.

Using the relative location method of Westaway (1987a), we (1987) established a preferred position for the 1980 mainshock nucleation point at location 4 in table I, which is ~9 km toward azimuth S71° E from our location for the aftershock. This relative location used *P*-wave arrival times from 63 regional and teleseismic stations that reported both events. We (1987) independently located the mainshock nucleation point directly using *P*-wave arrival times at 32 regional stations, determining location 3 in table I, which is within 2 km of location 4 (their formal standard error ellipses overlap – see fig. 3 of Westaway and Jackson, 1987). However, this direct location method is less reliable, partly because of the uneven station distribution (the shape of Italy causes most regional stations to be either to the northwest – the majority – or the southeast) and partly because, unlike the relative location method, it assumes no lateral variations in seismic velocity. Given the station distribution, displacing this mainshock nucleation point southeastward would adjust the estimated mainshock origin time slightly earlier, closer to the times that we deduce in this study (table I).

The US National Earthquake Information Service (NEIS) epicentre for the mainshock is ~15 km north of our (1987) preferred epicentre. As for the ISC and NEIS aftershock locations, its relatively late origin time is explicable as a result of systematic northward mislocation. The ISC mainshock location is not only too far north (which, on its own, would make the origin time late) but also is fixed at the Earth's surface, rather than at the more realistic ~10 km depth (which, on its own, given the downward propagation of *P*-wave ray paths from it, would make the origin time early). These two sources of systematic error in origin time for this ISC location largely cancel, giving an origin time very close to that for our (1987) location using regional stations (location 3 in table I).

2.2. *Revised location method*

As was shown by Westaway (1987a), if two earthquakes have the same focal depth, then their relative *P*-wave arrival time will vary sinusoidally with ray path azimuth, and is proportional to their separation. For a given separation and ray path azimuth, relative arrival time also varies in proportion to the sine of take-off angle relative to the downward vertical. Figure 1 shows a typical variation of take-off angle against epicentral distance for a crustal earthquake. This angle remains almost constant, in this case at (58÷59)°, out to

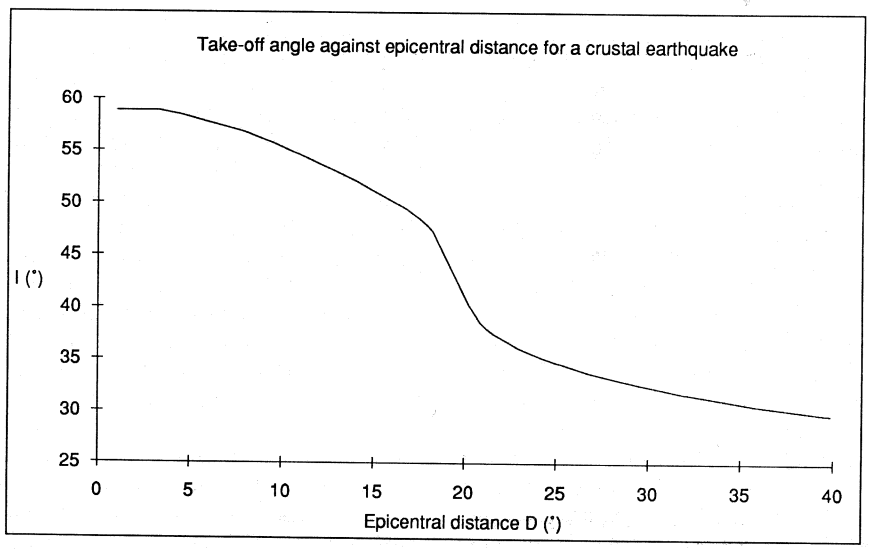

Fig. 1. Graph of take-off angle against epicentral distance, calculated using Herrin (1968) *P*-wave travel-time tables for an earthquake source at 10 km depth in 33 km thick crust in which *P*-wave velocity is 6.8 km s^{-1}.

distance ~800 km or ~7°, because the first *P*-wave arrival in this distance range, the *Pn*-phase, is refracted along the Moho. Moving to slightly greater distances, the take-off angle decreases more rapidly, from ~58° to ~54° over ~7° to 12° distance, as ray paths start to dive gently into the upper mantle. Rays travelling to greater distances will dive progressively more steeply, with the rapid variation in take-off angle around 20° distance associated with rays that bottom out deeper in the upper mantle, where *P*-wave velocity increases sharply with depth.

The method proposed here uses relative arrival time at close stations to which the uppermantle part of the ray path is subhorizontal. For these stations and for a pair of earthquakes with horizontal separation x, the peak-to-peak amplitude Δt_a of the expected sinusoidal variation of relative arrival time against ray path azimuth can readily be shown to equal $2\,x\,/\,v_m$, where v_m, ~8 km s^{-1}, is the *Pn*-wave velocity in the uppermost mantle.

P-wave arrival times and other data from all seismograph stations within 12° epicentral distance that recorded both the mainshock and the 8 December aftershock, and which are used in this relative location, are listed in table II of Westaway (1992). The next-nearest station that recorded both events was 19° distant, and only 10 common stations were identified between 19° and 40°. The 12° cutoff in distance was thus not only dictated given fig. 1, but is also a natural break in the available data. As noted above, the take-off angle to a station at 12° distance will be ~54°, not 59° for the *Pn*-phase. However, because the ratio of sin(59°)/sin(54°) is only ~1.06, treating all data as though they had the same take-off angle will introduce a maximum systematic error of only ~6% in predicted separation. For this pair of earthquakes this systematic error is unimportant, because random errors in arrival times at many stations appear to be ~1 s. With Δt_a later shown to be ~4 s, some individual relative arrival time data thus have ~25% random errors, which exceed the systematic error.

2.3. *Results*

Most relative *P*-wave arrival times Δt are consistent with a sinusoidal azimuthal variation, confirming the expected nonzero horizontal separ-

ation of the two events. At a few stations relative arrival times differ from those observed at other stations at similar azimuths. These discrepant data are most likely caused by errors in picking arrival times for one or other event, or errors in seismograph timing.

Figure 2a) shows the data that remain after the most obviously discrepant data are excluded. Their distribution is fairly diffuse, including apparent outlying points from FIR, GAP, ORI and SRO. The low Δt at GAP is caused by a +3.1 s residual for the aftershock. Its *P*-wave arrival time is likely to have been picked late. The high value at FIR is caused by a +3.7 s residual for the mainshock. This is likely to be either a picking or a timing error. Although the cause of the outlier at SRO is difficult to judge, this point lies so far away from others for stations at similar azimuths that it can be reasonably regarded as erroneous. However, there is nothing about the point for ORI, either considering its residuals or its consistency with neighbouring points, that clearly establishes it as erroneous. Figure 2b) contains the same data as 2a), except that it omits the points for FIR, GAP and SRO that can be reasonably excluded: 46 data are plotted altogether, substantially fewer than the 63 used by us (1987). 11 of the excluded data are from the distance range $(1 \div 12)°$, having been identified as unreliable in the above analysis. The other data, from more distant stations, are not considered here: they correspond to the distance $(19 \div 39)°$ where the take-off angle varies strongly and ray paths are typically steeper, making relative arrival time less sensitive to the separation of the two events.

It can be reasonably assumed *a priori* that the sine curve to be fitted to the data in fig. 2b) has phase ~210°, corresponding to a mainshock nucleation point ~S60°E of the aftershock. Two important constraints restrict the range of curves that can be reasonably fitted by eye. First, the information available *a priori* suggests that the second part of relative origin time is $\sim(12.0 \div 12.5)$ s (table I). Any sine curve fitted should thus oscillate about a baseline at Δt $(12.0 \div 12.5)$ s. Second, the trend of the numerous data from the northwest quadrant requires the peak of the fitted sine curve to be at Δt ~14.25 s. However, because fewer data are available from stations to the south, the trough of the sine curve is less well defined. If this curve is fitted through the point from ORI (curve A), its trough is at Δt ~9.75 s. Its baseline is then at $\Delta t = 12.0$ s and the peak-to-peak amplitude is 4.5 s corresponding to 18 km separation. If a sine curve is fitted instead through the trend of the data from the northeastern quadrant, its trough is at Δt ~10.75 s. Its baseline is then at $\Delta t = 12.5$ s and the peak-to-peak amplitude is 3.5 s corresponding to 14 km separation. Without making a value judgement as to the relative reliability of station ORI (in southern Italy) against the stations in the northeastern quadrant (which are mostly in Eastern Europe), analysis cannot proceed further.

Coordinates of mainshock nucleation-point locations corresponding to curves A and B in fig. 2b) are listed in table I. Westaway (1992) discusses in detail why this revised method gives a substantially different result from our (1987) location, even though the data set used is largely the same.

3. Implications for the sequence of fault ruptures

3.1. *The Carpineta, Marzano, and Picentini faults*

We (1987) suggested that the early part of the teleseismic body wave records began with a fault rupture subevent lasting 4 s, with $M_0 = 2.5 \times 10^{18}$ Nm, followed by a second subevent, which initiated 2.5 s later, was concentrated ~8 km northwest of the first, and had seismic moment $M_0 = 6.2 \times 10^{18}$ Nm. A third subevent, which initiated 6.8 s after, and 14 km northwest of, the first, had $M_0 = 4.5 \times 10^{18}$ Nm and duration 4.6 s. In view of our (1987) preferred position of the fault rupture nucleation point near a downdip projection of the Marzano fault, we (1987) suggested that the initial rupture occurred on the Marzano fault, and the second and third ruptures occurred on the Picentini fault. Nucleation point positions A and B are $\sim(5 \div 9)$ km southeast of our (1987) preferred location 4. They are near a downdip projection of the Carpineta scarp, where surface faulting was first reported by Pantosti and Valensise (1990a): A is near a downdip projection of the southeast end of this fault, and B is near a

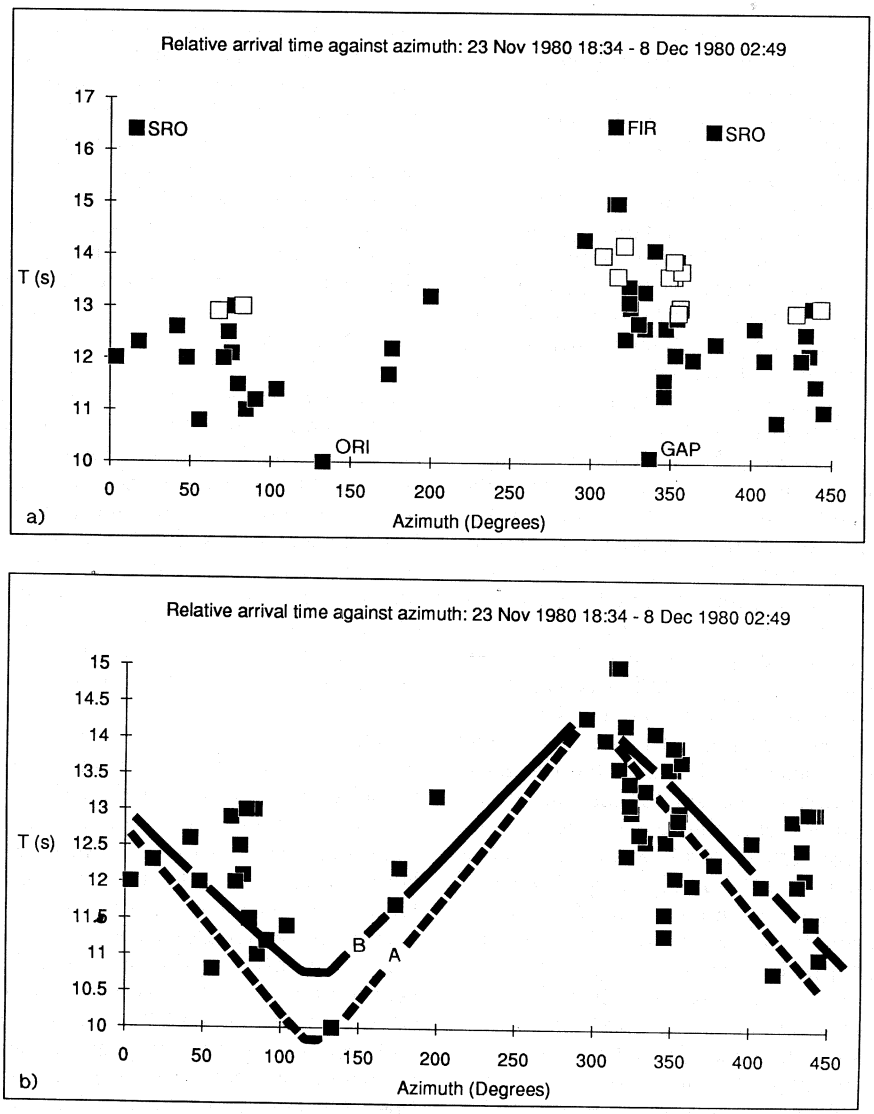

Fig. 2. Plots of relative arrival time against azimuth for the mainshock and the December 8 aftershock, showing lateral variations that are primarily caused by the mainshock nucleation point being offset southeast of the aftershock hypocentre, but which are also affected to some extent by timing and picking errors. a) Including all data from the distance range (1÷12)° except data that are obviously discrepant. Data where both the mainshock and aftershock show large but similar residuals are indicated using open symbols. b) Excluding data from FIR, GAP and SRO, and showing curves A and B fitted by eye through the remaining data. Note that azimuths (0÷90)° and (360÷450)° are equivalent. Curve B matches better the data from this azimuth range (which is repeated), whereas curve A matches better the data from azimuth range ~(300÷360)° (which is only displayed once). Repetition of the fraction of the data that matches curve B better gives the misleading impression (which should be discounted) that overall the data matches curve B better than curve A. The azimuth range (0÷90)° is repeated to facilitate comparison with adjacent azimuths.

downdip projection of its northwest end. Location A thus requires that mainshock rupture nucleated on the Carpineta fault (fig. 3), but B is consistent with either the Marzano fault or the Carpineta fault having ruptured first.

For a fault rupture with known downdip length D and along-strike length L, with average slip u in rock with shear modulus μ, seismic moment M_0 can be estimated as the product μuLD. Given the typical ~1 m of vertical slip observed in the field on the Marzano fault, and given its ~10 km length, ~10 km vertical extent, and likely shear modulus ~30 GPa, we (1987) suggested that the expected seismic moment released on it would be $\sim 3 \times 10^{18}$ Nm, apparently confirming our (1987) waveform modelling. This reasoning and the relative positions of the second and third subevents led us (1987) to suggest that they both occurred on the Picentini fault. However, two principal factors invalidate this comparison. First, as already noted, the work by Ward and Barrientos (1986) shows that the slip at the Earth's surface on a normal fault with ~60° dip embedded in an elastic halfspace is roughly half the maximum slip on the fault at depth. The average slip on each fault that slipped in the 1980 earthquake is taken as ~1.7 times the slip at the Earth's surface, to account for this factor in a manner that is approximately consistent with Ward and Barrientos (1986). Second, but of less importance, with 60° fault dip, u equals the vertical slip divided by sin(60°) and H equals the brittle layer thickness divided by sin(60°). Allowing for both these effects adjusts the field estimate for seismic moment released on the Marzano segment to $\sim(6 \div 7) \times 10^{18}$ Nm, similar to the seismic moment released in the second subevent in our (1987) teleseismic waveform modelling. With vertical slip 0.5 m on the Carpineta fault (Pantosti and Valensise, 1990a), this reasoning predicts $< \sim 3 \times 10^{18}$ Nm seismic-moment release there, similar to the seismic moment released in the first subevent of our (1987) teleseismic waveform modelling.

Comparison of the seismic moments observed in the first two subevents identified in our (1987) teleseismic waveform modelling with the values predicted from field evidence suggests that the first ruptured the Carpineta fault and the second ruptured the Marzano fault, regardless of whether location A or B is preferred. If location A is correct, the initial rupture nucleated near the southeast end of the Carpineta fault and propagated northwest. Alternatively, if location B is accepted, the initial rupture propagated southeast along the Carpineta fault. It thus remains unclear at this stage whether the Carpineta rupture propagated northwestward or southeastward. The relative position of the third subevent from our (1987) teleseismic waveform modelling suggests that it should be associated with the Picentini scarp (fig. 3 and 4).

Table III compares field estimates for the seismic moment released on the Carpineta, Marzano, and Picentini faults with seismic moments from our (1987) waveform modelling. Field estimates are calculated as $\mu L\,(H / \sin\delta)\,(c\,u_z / \sin\delta)$, where μ is the assumed shear modulus (30 GPa), L and H are the along-strike length and vertical extent of the fault, u_z is the vertical slip, δ is the dip of the fault, and the factor c of ~1.7 approximately converts slip at the Earth's surface to average slip. The two sets of seismic-moment estimate match well. The separation of the mid points of the Carpineta and Marzano faults in the field (9 km) also approximates the northwestward offset between the first two subevents in our (1987) teleseismic waveform modelling (8 km).

Fault ruptures in the brittle upper crust typically propagate at ~3 km s^{-1}. Rupture of the ~8 km distance northwestward along the Carpineta fault from nucleation point 1 in fig. 3, which is consistent with location A, would be expected to take ~2.7 s, which is similar to the 2.5 s interval between the first and second subevents in our (1987) waveform modelling. If location A is preferred, rupture thus propagated continuously northwestward from the Carpineta fault to the Marzano fault. In contrast, if location B were adopted instead, the similarity of the delay between the first two subevents observed teleseismically and the time required to rupture the Carpineta fault is a coincidence. Although not conclusive, my preference is thus that the initial rupture nucleated at the southeast end of the Carpineta fault (location A), because as well as matching the field and seismological estimates for seismic moment this choice can also explain the delay between the first and second subevents that are observed teleseismically.

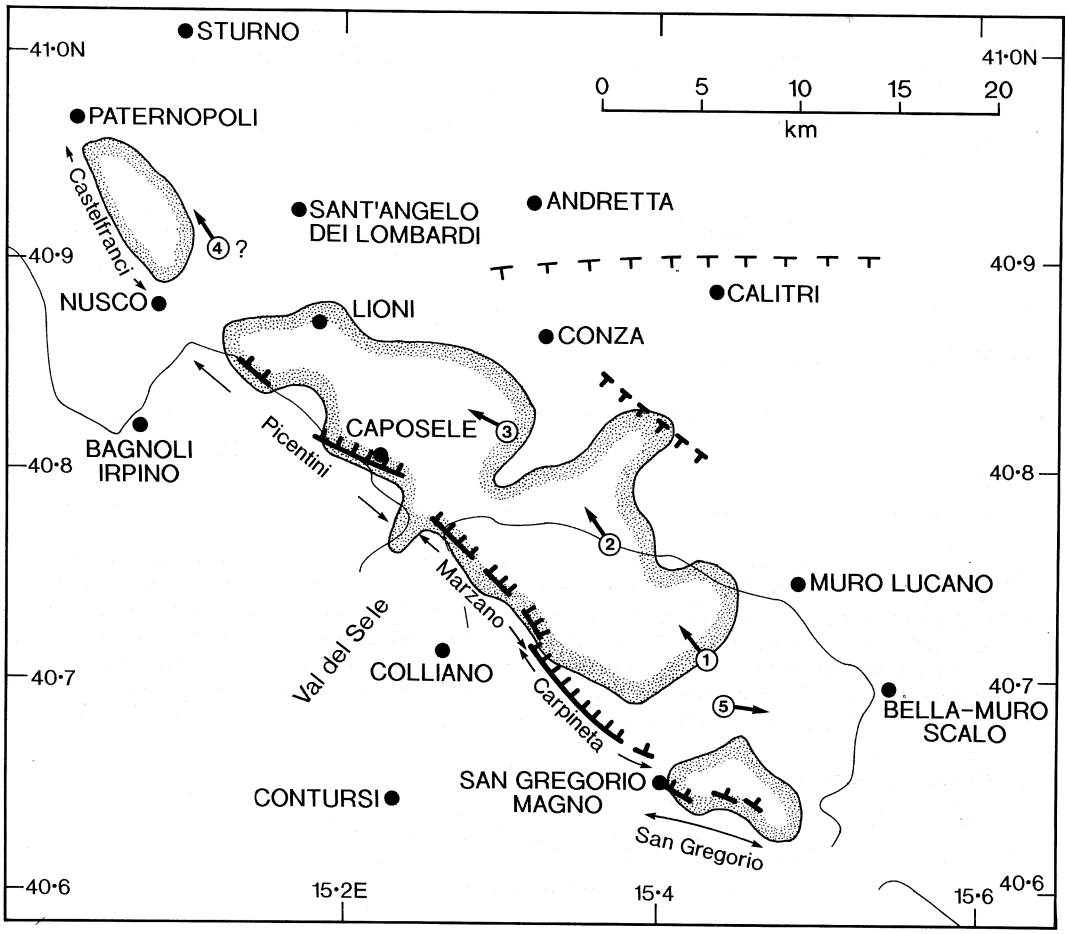

Fig. 3. Summary map of the epicentral area indicating my preferred working hypothesis for the 1980 earthquake. Numbered arrows indicate suggested nucleation points and rupture directions for the four or five subevents that ruptured steep NE-dipping normal faults. Thick lines denote observed surface faulting, with hanging wall ticks, from Pantosti and Valensise (1990a). Dashed thick line with ticks indicates the position of the antithetic fault that Bernard and Zollo (1989) suggested ruptured in the 40 s subevent. Dashed thin line with ticks denotes an apparent SSW-dipping normal fault at the north margin of the Cairano Pliocene sedimentary basin (see fig. 25 and 26 of Westaway and Jackson, 1987). This fault appears to have had no involvement in the 1980 earthquake. Shading enclosed by a thin line denotes the area of most intense aftershock activity, simplified from Westaway (1985) and Westaway and Jackson (1987). Its northwestern limit is outside the temporary seismograph network, and is thus poorly constrained. Although stations were deployed relatively sparsely to the southeast, the marked southeastern limit of aftershock activity lies well within the network, and is thus well defined. The thin line denotes the northeast limit of the Campania- Lucania carbonate platform, also from Westaway and Jackson (1987). Note the alignment of the southwest edge of the aftershock area with the surface faulting on the Marzano fault (first noticed by Westaway and Jackson, 1984), and the similar alignment on the parts of the Picentini fault where surface faulting is exposed. See text for discussion.

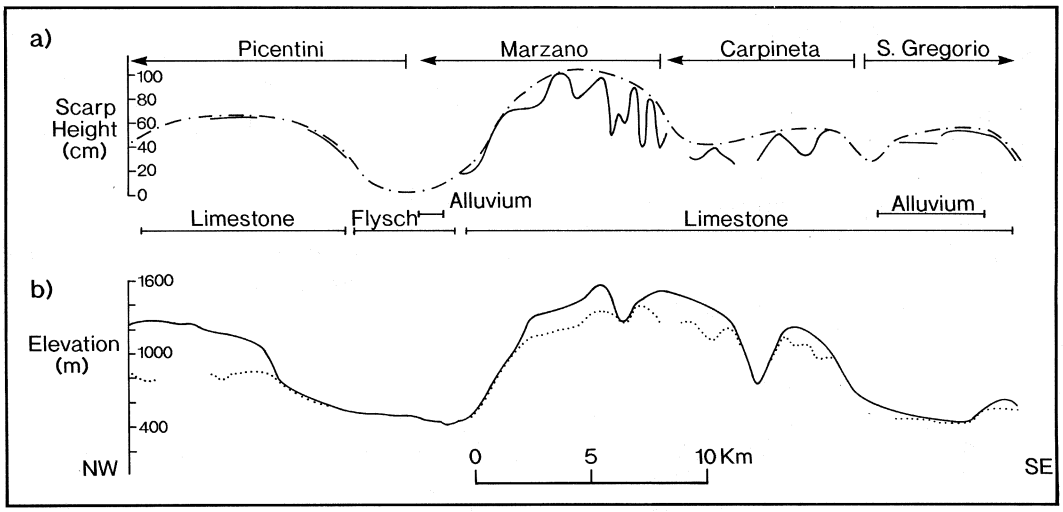

Fig. 4. Profiles of scarp height (a)) and topography (b)) for the San Gregorio, Carpineta, Marzano, and Picentini scarps. In a) the solid curve denotes scarp observations, and the dot-dashed curve estimates original scarp height before degradation, providing a measure of u_z, the vertical slip at the Earth's surface, at each locality. In b) the dotted curve is scarp elevation above sea level, and the solid curve is elevation above sea level of the crest of the footwall escarpment near the scarp. The difference between these two curves gives an estimate of total throw across each fault. Note that although the Marzano and Picentini scarp heights in 1980 have ratio ~2:1, footwall escarpment heights are roughly equal. Redrawn from fig. 6 of Pantosti and Valensise (1990a).

Table III. Seismic-moment release on individual normal faults.

Number + Name	L (km)	u_z (m)	$M_0(F)$ (10^{18} Nm)	$M_0(S)$ (10^{18} Nm)	ϕ (°)	ψ	t (s)	M_W
Ruptures on faults dipping northeast at ~60°								
1. Carpineta	9	0.5	2.4	2.5	315	NW	0	6.2
2. Marzano	10	1.0	6.7	6.2	315	NW	2.5	6.5
3. Picentini	12	0.6	4.9	4.5	300	NW	6.8	6.4
(4. Castelfranci	~7	~0.5	~2.4	~2.0	330	NW	~12	6.2)
5. San Gregorio	7	0.5	2.4	(2.0)	300	SE	~14	6.2
Total	40÷48		16.4÷18.8	15.2÷17.2				
Rupture dipping northeast at 20° at base of brittle layer								
20 s subevent				4.0	315	NE	~20	6.4
Rupture on fault dipping southwest at ~70°								
40 s subevent				3.0	135	?	~40	6.3
Total				22.2÷24.2				

L is the along-strike length; u_z is the vertical slip, observed or estimated, at the Earth's surface; $M_0(F)$ and $M_0(S)$ are field and seismological estimates for seismic moment; ϕ is the strike; ψ is the rupture direction; t is the nucleation time after the initial rupture initiated; and M_W is the moment-magnitude calculated from M_0 using Hanks and Kanamori's (1979) equation. $M_0(F)$ estimates are for 60° dip and 10 km vertical extent for each normal fault, and assume the ratio c of slip at the Earth's surface to the average slip is 1:1,7. $M_0(S)$ values are from Westaway and Jackson (1987), except for the Castelfranci and San Gregorio ruptures that are discussed in the text. If the Carpineta and Marzano ruptures are counted together, they have M_W = 6.6.

The following preferred description of the first three subevents is consistent with location A for the fault rupture nucleation point, the field evidence of faulting, and the teleseismic waveform modelling. Fault rupture initiated at or near the southeast end of the Carpineta fault and propagated northwestward, releasing ~2.5×10^{18} Nm seismic moment with ~0.5 m of vertical slip at the Earth's surface and taking ~2.5 s to reach the northwest end of this fault. Rupture then propagated without interruption onto the Marzano segment, releasing ~6.5×10^{18} Nm of seismic moment with ~1 m of vertical slip at the Earth's surface. Rupture would have thus taken ~6.3 s to cover the total 19 km length to the northwest end of the Marzano fault. At this point the rupture paused for ~0.5 s, before a second rupture initiated on the Picentini fault, causing ~0.6 m vertical slip and releasing ~4.5×10^{18} Nm seismic moment, probably dying out where the uniform northwestward trend of the Picentini range front is interrupted by a southwestward step near Nusco (see fig. 3 and Plate 1 of Westaway and Jackson, 1987).

3.2. *The 40 s subevent*

We (1987) suggested, on the basis of the timing of ground acceleration, that the 40 s subevent nucleated ~(8÷16) km from the first subevent, at an azimuth between north and N40°E. We (1987) adopted the nominal position ~12 km north of the nucleation point of the first subevent for our (1987) waveform modelling. Bernard and Zollo (1989) estimated the separation of the first and 40 s subevents as ~8 km toward N10°E, which lies within the broader region suggested by us (1987). They (1989) also noted seismological observations, and observations of elevation change and geomorphology, which they suggest require that the 40 s subevent involved slip on a steep SW dipping normal fault that passed a few kilometers south of Calitri (fig. 3). These pieces of evidence appear reasonable, and indicate that the 40 s subevent occurred on a steep normal fault with SW dip, which is situated opposite the Marzano fault, the two faults being ~11 km apart at the Earth's surface but adjoin at the base of the brittle layer (fig. 5).

Tables II and IV investigate the timing of seismic phases recorded by accelerographs, given the revised nucleation point A for the initial fault rupture, with the 40 s subevent assumed to have occurred on the SW-dipping normal fault in fig. 3. With the exception of the *S*-wave from the 40 s subevent at Bagnoli Irpino (which we (1987) picked late, as Bernard and Zollo (1989) noted), and the *S*-wave from the initial rupture at Sturno (which we (1987) also picked late), the two interpretations are very similar. Most relative arrival times are consistent with the initial and 40 s subevents being in these revised positions. The main differences compared with previous interpretations are, first, that most data support the origin time for the 40 s subevent at > ~40 s, not ~(38÷39) s, after the initial rupture nucleated. Second, timing consistency is greatest if energy from the 40 s subevent was radiated from near where this SW-dipping normal fault reaches the Earth's surface, rather than from near its downdip limit farther southwest. No accelerograph station listed in tables II and IV is southeast of the source region. This is because the initial fault rupture triggered none of the accelerographs in that quadrant (Bernard and Zollo, 1989), presumably because it radiated most energy towards its northwestward direction of propagation, as is expected.

4. Along-strike extent of faulting and its timing

Opinions have differed strongly as to the along-strike extent of faulting in the 1980 mainshock. Pantosti and Valensise (1990a) reported that there was no evidence of surface faulting either northwest of the Picentini range front or southeast of the San Gregorio scarp, making the along-strike length of faulting ~40 km. In contrast, others who have modelled accelerograms of the 1980 mainshock have proposed much longer extents of faulting. For example, Suhadolc *et al.* (1988), Panza and Suhadolc (1989), Vaccari *et al.* (1990) and Harabaglia *et al.* (1990) have all suggested ~70 km total length. The southeastern limit of faulting is undoubtedly the southeastern limit of the San Gregorio rupture (*e.g.*, Pantosti and Valensise, 1990a), which coin-

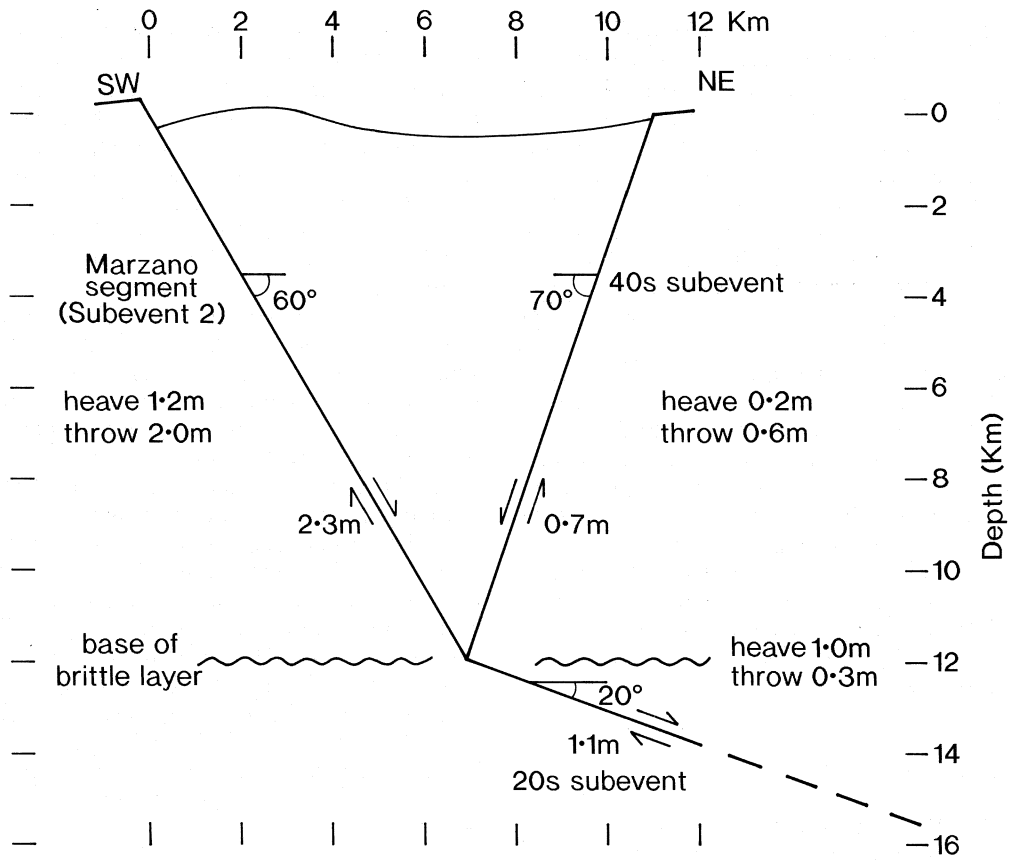

Fig. 5. Schematic cross-section across the Marzano fault and its associated antithetic fault ~11 km farther northwest, which appears to have ruptured in the 40 s subevent of the 1980 earthquake. Heave, throw and slip are estimates at depth and exceed those at the surface.

cides with the southeastward limit of concentrated aftershock activity (fig. 3). If the occurrence of fault rupture at Castelfranci is accepted, the northwestern limit of faulting is the northwestern limit of this rupture, and the overall along-strike length of faulting is ~50 km. This section discusses the San Gregorio and Castelfranci ruptures, which appear to bound the overall extent of faulting.

4.1. *The San Gregorio rupture*

The timing of slip on the San Gregorio fault remains problematical. We (1987) suggested, using teleseismic waveforms and timing of accelerograms, that it began 12.8 s after the first subevent nucleated. Our (1987) waveform analysis indicated a subevent with seismic moment 2×10^{18} Nm initiated 12.8 s after the initial subevent. Our (1987) analysis of the Brienza accelerogram led us to conclude that the San Gregorio fault ruptured at this time. However, this interpretation needs to be modified following the revision to the timing and nucleation point of the initial rupture. The field estimate for the seismic moment on the San Gregorio fault, only ~2×10^{18} Nm, is so small that, provided it ruptured within ~15 s of the first subevent, it can be concealed more or less anywhere within synthetic body-

Stn	R_0 (km)	R_{40} (km)	r_{40} (km)	R_{40}–R_0 (km)	r_{40}–R_0 (km)	ΔT_1 (s)	ΔT_2 (s)	$T_{40,1}$ (s)	$T_{40,2}$ (s)
BAG	32.5	27.6	27.8	-4.9	-4.7	-1.4	-1.3	40.7 ± 0.4	40.6 ± 0.4
BIS	33.9	27.9	23.6	-6.0	-10.3	-2.0	-3.4	37.5 ± 0.6	38.9 ± 0.6
BOV	59.9	53.5	48.3	-6.4	-11.6	-1.8	-3.3	39.4 ± 2.5	40.9 ± 2.5
CAL	22.0	17.5	9.3	-4.5	-12.7	-1.5	-4.2	37.5 ± 0.3	40.2 ± 0.3
MER	56.1	52.0	53.6	-4.1	-2.5	-1.2	-0.7	41.7 ± 1.3	41.2 ± 1.3
RIO	33.0	31.8	25.7	-1.2	-7.3	-0.4	-2.4	39.2 ± 1.5	41.2 ± 1.5
STU	42.8	35.8	32.8	-7.0	-10.0	-2.0	-2.9	40.2 ± 0.6	40.9 ± 0.6

Stn denotes the accelerograph station, as in table II. Station coordinates from table 2 of Bernard and Zollo (1989) are used. R_0 is the distance to the station from my preferred nucleation point for the initial rupture (A in table I). R_{40} is the distance to the station from my preferred downdip limit for the 40 s rupture (at 40.78°N, 15.37°E, 10 km depth). r_{40} is the distance to the station from my assumed point where the 40 s rupture reached the Earth's surface (at 40.82°N, 15.40°E). ΔT_1 and ΔT_2 are $(R_{40}–R_0)/V_S$ and $(r_{40}–R_0)/V_S$, where V_S is the assumed average S-wave velocity (see caption to table II). $T_{40,1}$ and $T_{40,2}$ are estimates of the interval between the initial and 40 s ruptures, obtained by adding ΔT_1 or ΔT_2 to preferred S_{40}–S_0 values from table II. Note that R_{40}–R_0 values calculated in this table agree well with independent estimates of R_{40}–R_0 and r_{40}–R_0 from the accelerograph timing, in table II. Note also the greater consistency of $T_{40,2}$ values, which require a ~40 s interval between the two ruptures.

Table IV. Deductions of relative position and timing of the initial and 40 s subevents.

wave seismograms, being overwhelmed by the larger Marzano and Picentini ruptures.

Brienza is 33 km from the initial rupture nucleation point A and ~43 km from the 40 s rupture. According to Bernard and Zollo (1989), the S-wave from the 40 s rupture arrived at Brienza (37.8 ± 0.2) s after the instrument triggered. Assuming velocity 3.5 km s^{-1}, travel times to Brienza are 9.4 s and 12.3 s for S-waves from the initial and 40 s ruptures. Assuming the 40 s rupture occurred 40 s after the initial rupture (consistent with tables II and IV), the delay between the S-wave from the initial rupture and the triggering of the Brienza accelerograph is thus 40 + 12.3 – 9.4 – 37.8 s or ~5 s. The S-wave from the San Gregorio rupture arrived at Brienza (9.5 ± 0.2) s after triggering, according to Bernard and Zollo (1989), or ~9 s according to us (1987). Origin time of this signal was thus ~9 + 5 s or ~14 s after the initial rupture nucleated if its source was near the nucleation point A, or ~1.5 s later if it originated beneath the central part of the San Gregorio fault. Faster S-wave propagation would adjust this origin time earlier.

This interpretation of the Brienza accelerogram suggests that the San Gregorio fault ruptured no later than ~(14÷16) s after rupture initiated on the adjacent Carpineta fault. The length of the San Gregorio fault is such that it requires only ~2 s to rupture throughout. It is thus incorrect to associate the rupture of the San Gregorio fault with the 20 s subevent observed teleseismically, which occurred ~(19÷27) s after the initial rupture. In the absence of convincing evidence to the contrary it thus seems reasonable to return to our (1987) suggestion that the 20 s subevent observed teleseismically occurred on a low-angle surface at the base of the brittle layer, northeast of the Marzano fault. This position is directly beneath the steep SW-dipping fault that ruptured in the 40 s subevent (fig. 5). As already noted, seismic moment ~2×10^{18} Nm and moment magnitude M_W ~6.2 are expected for the San Gregorio rupture. Joyner and Boore's (1981) equation predicts peak horizontal ground acceleration (PHGA) ~1 ms^{-2} for M_W 6.2 at ~28 km distance. Observed PHGA at Brienza was ~1.5 ms^{-2} (*e.g.*, Bernard and Zollo, 1989), in reasonable agreement.

Using Bernard and Zollo's (1989) slower velocity structure, S-wave travel time to Brienza is 9.4 s for the San Gregorio rupture, and would be ~15 s and ~11 s from the revised hypocentres for the initial and 40 s subevents. The delay between the S-wave from the initial rupture and the triggering of the Brienza accelerograph would be ~6 s, and the delay between the initial rupture and the San Gregorio rupture would thus be ~17 s: still too small to associate the San Gregorio rupture with the ~20 s subevent that we (1987) identified teleseismically.

4.2. *The Castelfranci rupture*

The Sturno accelerogram is potentially of crucial importance for the understanding of this earthquake. Observed PHGA exceeded 3 m s^{-2} (Westaway and Smith, 1989) ~(5÷6) s after this instrument triggered. Sturno is ~15 km from the closest point on a surface projection of the Picentini fault and ~28 km from the closest point on a surface projection of the Marzano fault (fig. 3). If the Marzano rupture had occurred in isolation, its seismic moment and equivalent magnitude (table III) would be expected to cause barely ~1 ms^{-2} of PHGA at this distance. Similar PHGA would also be expected if the Picentini rupture had occurred in isolation (using Joyner and Boore's 1981 equation: see Westaway and Smith, 1989). Given this discrepancy, we (1987) suggested that the high PHGA at Sturno may have been a directivity effect of the rupture on one or both of these faults propagating northwestward towards Sturno.

Subsequent modelling of ground acceleration (*e.g.*, Siro and Chiaruttini, 1989; Vaccari *et al.*, 1990; Harabaglia *et al.*, 1990) indicates, in contrast, that PHGA at Sturno was caused by a relatively small fault rupture nearby. The Castelfranci fault (fig. 3), which is identified by its aftershock cluster, seems a strong candidate for this nearby fault rupture, with the closest point on its surface projection ~6 km from Sturno. The Castelfranci aftershock cluster has similar dimensions to the cluster around the San Gregorio fault farther southeast. Assuming the Castelfranci rupture involved the same slip and fault dimensions as at San Gregorio, it would have also released seismic moment ~2×10^{18} Nm, equivalent to M_W ~6.2 (using Hanks and Kanamori's 1979 equation). With this moment magnitude and distance to Sturno, PHGA ~3 ms^{-2} is predicted using Joyner and Boore's (1981) equation, as is observed.

The 6.8 s initiation time and 4.6 s duration for the Picentini rupture suggest that it died out at the northwest end of the Picentini fault ~11.4 s after the first rupture initiated. If the poorly-resolved 12.8 s subevent that we (1987) identified is associated with the Castelfranci fault (instead of with the San Gregorio fault, as we (1987) originally suggested), then its timing suggests a ~1.4 s delay at the northwest end of the Picentini fault, before propagation resumed. According to Bernard and Zollo (1989), the *S*-wave from the initial rupture arrived at Sturno 2.3 s after the instrument triggered. With Sturno ~43 km from nucleation point A and ~10 km from the likely position at depth of the Castelfranci rupture, the *S*-wave from this rupture would be expected to have a travel time ~(43 km – 10 km)/ 3.5 km s^{-1} less, or ~9.4 s less, than the signal from the initial rupture. Assuming that the strong signal starting ~5 s after the Sturno instrument triggered (which we (1987) mistakenly picked as the *S*-wave arrival from the initial fault rupture) was the *S*-wave from the Castelfranci rupture, this began ~5 + 9.4 –2.3 s or ~12.1 s after the initial rupture, consistent with the tentative reinterpretation of our (1987) waveform modelling. I hope in future to confirm this reinterpretation by additional waveform modelling. However, this is likely to be difficult, because the Castelfranci and San Gregorio ruptures (starting ~12 s and ~14 s after the initial rupture) appear to have occurred so close together in time.

5. Discussion

5.1. *Normal fault morphology*

Some people (*e.g.*, Ambraseys and Tchalenko, 1972) have suggested that the sense of stepping along fault scarps correlates with the sense of the strike-slip component of slip: a left-lateral component is associated with rightward stepping. The Carpineta and Marzano scarps strike at ~315° and typically show stepping to the right every few hundred metres or more (Westaway and Jackson, 1984, 1987; Pantosti and Valensise, 1990a). We (1984, 1987) described one locality on the Marzano fault where striations on an exposed limestone surface indicate a small component of left-lateral slip. Such a component is supported by our (1987) first-motion focal mechanism, which had slip vector azimuth N37°E (Westaway *et al.*, 1989), and by our (1987) teleseismic waveform modelling.

Despite substantial variations in fault strike, slip vector azimuth remained roughly constant during the 1984 Lazio-Abruzzo earthquake sequence in central Italy (Westaway *et al.*, 1989). It seems reasonable to assume that it remained

constant in the Irpinia sequence of ruptures also. The San Gregorio scarp has typical strike ~300°, and, assuming the same slip vector azimuth, a component of right-lateral slip is expected instead. Strands of the discontinuous Picentini scarp have typical strike ~300° too, and a component of right-lateral slip is thus also expected there. The suggested Castelfranci fault farther NW has strike ~(320÷330)° instead, which would predict a greater proportion of left-lateral slip that was observed on the Marzano scarp. On both the Carpineta-Marzano and San Gregorio scarps, the observed stepping sense is thus as expected, given the observed or expected sense of the strike-slip component.

5.2. *Extent of «missing» seismic moment*

Some people (*e.g.*, Pantosti and Valensise, 1990a) have noted apparent discrepancies between the total scalar seismic moment of the 1980 earthquake, which is ~26×10^{18} Nm (Westaway and Jackson, 1987) and the sum of field and seismological estimates for seismic moment of individual fault ruptures (table III). The sum of seismic moments for the three relatively well-documented subevents (Carpineta, Marzano and Picentini) is ~$(13.2\div13.6)\times10^{18}$ Nm. Allowing ~2×10^{18} Nm for each of the ruptures at San Gregorio and Castelfranci, total scalar seismic moment released on NE-dipping normal faults was ~17.6×10^{18} Nm. With 7×10^{18} Nm additional seismic-moment released in the 20 s and 40 s subevents, total scalar seismic moment rises to ~24.6×10^{18} Nm, within 5% of the expected amount. Seismic-moment estimates from teleseismic waveform modelling are inherently uncertain by ~20% (*e.g.*, Westaway and Jackson, 1987). Furthermore, the uncertainty as to whether a 10 km – or 12 km – deep base of the brittle layer should be used in field estimates of seismic moment also causes ~20% uncertainty. The 5% discrepancy between the overall scalar seismic moment and the estimates based on individual subevents is thus not significant, and there are thus no grounds for suggesting that any additional fault rupture occurred elsewhere. Given these ~20% margins, there is no need for slip on the Castelfranci fault to match the expected seismic moment. However, the aftershock cluster there, the results from the ground acceleration modelling, and the tentative reinterpretation of our (1987) teleseismic waveform modelling, support the existence of such a fault rupture.

5.3. *Comparison with waveform studies of ground acceleration records*

The interpretation of the 1980 earthquake summarized in table III and fig. 3 is based on teleseismic waveform modelling and analysis of arrival times of seismic phases. It indicates a sequence of NW-propagating fault ruptures lasting ~15 s and covering > ~40 km, with a <~10 km long SE-propagating rupture farther southeast, which started ~14 s after the NW-propagating ruptures began. It is reasonably consistent with recent independent waveform studies of accelerograms. Its overall agreement with the results of Vaccari *et al.* (1990) is particularly striking, although they predicted a slightly longer duration, ~17 s, for the NW-propagating ruptures and modelled the SE-propagating rupture using sources mostly southeast of San Gregorio. This more distant southeast limit of faulting increased the overall fault rupture length to ~70 km.

Most published ground acceleration modelling treats virtually every aspect of this earthquake as a free parameter, including some (such as fault dip, strike, and slip sense) that are in fact tightly constrained. Hopefully, such modelling in future will instead use results for the overall fault rupture geometry that are based on independent evidence (such as that shown in fig. 3) to provide constraints, and will concentrate on resolving issues where genuine uncertainties remain (primarily, the detailed rupture timing). In this context, it should be noted that the northwest limit of the Castelfranci aftershock cluster is poorly resolved: at this extreme northwestward position aftershocks are beyond most of the temporary seismograph network and are thus poorly located (Westaway, 1985), and any real clustering there may have been smeared out by mislocation. The true northwest limit of the Castelfranci fault may thus be a few kilometres northwest of the position shown in fig. 3. However, it is most unlikely that the total length of faulting was ~70 km.

6. Conclusion

Reexamination of *P*-wave arrival time data to locate the nucleation point of the initial fault rupture in the 1980 Campania-Basilicata earthquake, using a revised relative location method, indicates that it was ~(5÷9) km southeast of our (1987) preferred position, and was probably near the southeast end of the Carpineta fault scarp. The first three fault rupture subevents that were resolved in our (1987) teleseismic waveform modelling correspond to northwestward rupture on the Carpineta, Marzano and Picentini faults, which strike northwestward and dip northeast at ~60°, with typical vertical slip and seismic moment on each fault estimated in table III. Rupture propagation appears to have experienced no delay at the northwest end of the Carpineta fault, but was delayed by ~0.5 s at the structural discontinuity at the northwest end of the Marzano fault before resuming on the Picentini fault. This Picentini fault rupture probably died out at another structural discontinuity near Nusco, ~33 km from the initial nucleation point. Aftershock and ground acceleration evidence suggest a fourth NW-propagating fault rupture at Castelfranci, beyond the northwest end of the Picentini fault, which may have begun ~12 s after the initial rupture nucleated and thus ~1 s after rupture reached the northwest end of the Picentini fault. The San Gregorio surface faulting was probably caused by a fifth rupture with similar orientation to the first three, which propagated southeast and initiated ~14 s after the Carpineta rupture. Two later subevents, ~20 s and ~40 s after the initial subevent nucleated, were associated with sources with different orientations. A previous suggestion that the 20 s subevent occurred on the San Gregorio fault is not supported. The 20 s and 40 s subevents appear instead to have both occurred northeast of the Marzano fault: the 20 s one apparently involved a low-angle rupture at the base of the brittle upper crust, whereas the 40 s one appears to have involved slip on a steep SW-dipping normal fault, the geometrical relationship of these faults being shown in fig. 3-5. Taken together, these 6 or 7 subevents account for the total scalar seismic moment of the earthquake.

REFERENCES

AMBRASEYS, N.N. and J.S. TCHALENKO (1972): Seismotectonic aspects of the Gediz, Turkey, earthquake of March 1970, *Geophys. J. R. Astron. Soc.*, **30**, 229-252.

ARCA, S., V. BONASIA, R. GAULON, F. PINGUE, J.C. RUEGG and R. SCARPA (1983): Ground movements and faulting mechanism associated to the November 23, 1980 southern Italy earthquake, *Boll. Geod. Sci. Affini*, **42**, 137- 147.

BERNARD, P. and A. ZOLLO (1989): The Irpinia (Italy) 1980 earthquake: detailed analysis of a complex normal faulting, *J. Geophys. Res.*, **94**, 1631-1647.

EYIDOGAN, H. and J.A. JACKSON (1985): A seismological study of normal faulting in the Demirci, Alasehir and Gediz earthquakes of 1969-70 in western Turkey: implications for the nature and geometry of deformation in the continental crust, Geophys. J. R. Astron. Soc., **81**, 569-607.

HARABAGLIA, P., P. SUHADOLC and G.F. PANZA (1990): Rupture process dynamics from inversion of accelerometric data, in *Preprints of the Proceedings of the International Meeting «Irpinia Dieci Anni Dopo», Sorrento, November 1990* (Istituto Nazionale di Geofisica, Roma), pp. 73-78.

HANKS, T.C. and H. KANAMORI (1979): A moment-magnitude scale, *J. Geophys. Res.*, **84**, 2348-2350.

HERRIN (1968): 1968 Seismological tables for *P*-phases, *Bull. Seismol. Soc. Am.*, **58**, 1193-1241.

JOYNER, W.B. and D.M. BOORE (1981): Peak horizontal acceleration and velocity from strong-motion records including records from the 1979 Imperial Valley, California, earthquake, *Bull. Seismol. Soc. Am.*, **71**, 2011-2038.

PANTOSTI, D. and G. VALENSISE (1990a): Faulting mechanism and complexity of the November 23, 1980, Campania-Lucania earthquake, *J. Geophys. Res.*, **95**, 15319-15342.

PANTOSTI, D. and G. VALENSISE (1990b): Source geometry and long term behavior of the 1980 fault based on field geologic observations, in *Preprints of the Proceedings of the International Meeting «Irpinia Dieci Anni Dopo», Sorrento, November 1990* (Istituto Nazionale di Geofisica, Roma), pp. 45-50.

PANZA, G.F. and P. SUHADOLC (1989): Realistic simulation and prediction of strong ground motion, in *Computers and Experiments in Stress Analysis*, edited by G.M. CARLOMAGNO and C.A. BREBBIA (Springer-Verlag, Berlin), pp. 77- 98.

POSTPISCHL, D. (1985): Atlas of isoseismal maps of Italian earthquakes (Consiglio Nazionale delle Ricerche, Roma).

SIRO, L. and C. CHIARUTTINI (1989): Source complexity of the 1980 southern Italian earthquake from the analysis of strong-motion *S*-wave polarization, *Bull. Seismol. Soc. Am.*, **79**, 1810-1832.

SUHADOLC, P., F. VACCARI and G.F. PANZA (1988): Strong motion modelling of the rupturing process of the November 23, 1980, Irpinia earthquake, in *Seismic Hazard in Mediterranean Regions*, edited by J. BONNIN (European Community, Brussels), pp. 105-128.

VACCARI, F., P. SUHADOLC and G.F. PANZA (1990): Irpinia, Italy, 1980 earthquake: waveform modeling of strong motion data, *Geophys. J. Int.*, **101**, 631-647.

WARD, S.N. and S.E. BARRIENTOS (1986): Inversion for slip distribution and fault shape from geodetic observations of the 1983 Borah Peak, Idaho, earthquake, *J. Geophys. Res.*, **91**, 4909-4919.

WESTAWAY, R. (1985): Active tectonics of Campania, southern Italy, PhD thesis, University of Cambridge.

WESTAWAY, R. (1987a): The Campania, southern Italy, earthquakes of 1962 August 21, *Geophys. J. R. Astron. Soc.*, **90**, 375-443.

WESTAWAY, R. (1987b): Comment on «The southern Italy earthquake of 23 November 1980: an unusual pattern of faulting», by CROSSON, R.S., M. MARTINI, R. SCARPA and S.C. KEY, *Bull. Seismol. Soc. Am.*, **77**, 1071-1074.

WESTAWAY, R. (1992): Revised nucleation point and fault rupture geometry for the 1980 Campania-Basilicata earthquake in southern Italy, *Geophys. J. Int.*, **109**, 376-390.

WESTAWAY, R. and J.A. JACKSON (1984): Surface faulting in the southern Italian Campania-Basilicata earthquake of 23 November 1980, *Nature*, **312**, 436-438.

WESTAWAY, R. and J.A. JACKSON (1987): The earthquake of 1980 November 23 in Campania-Basilicata (southern Italy), *Geophys. J. R. Astron. Soc.*, **90**, 375-443.

WESTAWAY, R. and R.B. SMITH (1989): Strong ground motion in normal faulting earthquakes, *Geophys. J.*, **96**, 529-559.

WESTAWAY, R., R. GAWTHORPE and M. TOZZI (1989): Seismological and field observations of the 1984 Lazio-Abruzzo earthquakes: implications for the active tectonics of Italy, *Geophys. J.*, **98**, 489-514.